

## Article

# Holocene Evolution of Minor Mountain Lacustrine Basins in the Northern Apennines, Italy: The Lake Moo Case Study

Stefano Segadelli <sup>1</sup>, Kei Ogata <sup>2,\*</sup>, Marco Cocuccioni <sup>3</sup>, Stefano Gambini <sup>4</sup>, Luca Martelli <sup>1</sup>,  
Lionello F. Morandi <sup>5</sup> and Gabriele Oppo <sup>6</sup>

- <sup>1</sup> Geological, Soil and Seismic Survey, Emilia-Romagna Region, Viale della Fiera 8, 40127 Bologna, Italy; stefano.segadelli@regione.emilia-romagna.it (S.S.); luca.martelli@regione.emilia-romagna.it (L.M.)
- <sup>2</sup> Department of Earth Sciences, Environment and Resources, University of Naples Federico II, 80126 Naples, Italy
- <sup>3</sup> Freelance Researcher, Via dell'Ongaro 8, 21010 Cardano al Campo, Italy; lacucas85@gmail.com
- <sup>4</sup> Geologist Freelance, Cascina Tirogno 4/F, 27012 Certosa di Pavia, Italy; stefano.gambini@gmail.com
- <sup>5</sup> Competence Center Archaeometry—Baden-Württemberg, Eberhard-Karls-Universität Tübingen, Wilhelm Str. 14 56, 72074 Tübingen, Germany; lionello.morandi@uni-tuebingen.de
- <sup>6</sup> Geologist Freelance, Vicolo San Clemente 1, 43043 Borgo Val di Taro, Italy; gabrieleoppo.geo@libero.it
- \* Correspondence: kei.ogata@unina.it

**Abstract:** Sedimentary systems developed in small (<1 km<sup>2</sup>) mountain lacustrine basins represent high-resolution geological archives, able to record subtle climatic and tectonic signatures over historical times. The studied example from the Mt. Ragola ophiolitic massif in the Northern Apennines (Italy) allowed us to better understand the role of the different (neo)tectonic and climatic events on the development and distribution of large landslides and lakes/peat bogs during the last 10 kyrs. Implementing a multidisciplinary approach that includes detailed acquisition of bedrock, geomorphological, topographic, and geophysical data, we detected and mapped ridge splitting, trenches, closed depressions, double ridges, and counterscarps. These morphostructures are interpreted as relevant factors influencing the distribution of sediments in historical times by shifting the position of the local equilibrium point (i.e., erosion vs. deposition) and have been correlated to a combination of climatic (i.e., increased flood events) and tectonic (i.e., spatial-temporal clustering of seismic shocks) forcing, starting from the demise of the Little Ice Age in the mid-19th century to the present-day situation. This approach allowed us to better describe the current changes in the hydrologic cycle, reaching beyond the limits of historical instrumental data. Furthermore, allowing the recognition and dating of recent tectonic vs. gravitational deformations, it also constitutes an integrative method for assessing the local geological hazard.

**Keywords:** Northern Apennines; historical archives; geological events; high-resolution mapping; topographic lineament



**Citation:** Segadelli, S.; Ogata, K.; Cocuccioni, M.; Gambini, S.; Martelli, L.; Morandi, L.F.; Oppo, G. Holocene Evolution of Minor Mountain Lacustrine Basins in the Northern Apennines, Italy: The Lake Moo Case Study. *Geosciences* **2022**, *12*, 272. <https://doi.org/10.3390/geosciences12070272>

Academic Editors: Jesus Martinez-Frias and Juan Pablo Corella

Received: 12 April 2022

Accepted: 29 June 2022

Published: 5 July 2022

**Publisher's Note:** MDPI stays neutral with regard to jurisdictional claims in published maps and institutional affiliations.



**Copyright:** © 2022 by the authors. Licensee MDPI, Basel, Switzerland. This article is an open access article distributed under the terms and conditions of the Creative Commons Attribution (CC BY) license (<https://creativecommons.org/licenses/by/4.0/>).

## 1. Introduction

The reconstruction of the recent stratigraphic, tectonic, and morphological evolution and the characterization of the geological hazard are fundamental for safe and sustainable land management, especially in tectonically active zones. However, in many geological contexts, the traces of recent evolution are not always evident. This is the case of the Emilian Apennines, where the main geological units are made up of highly tectonized, easily erodible clayey complexes.

In this framework, small-scale (<1 km<sup>2</sup>), lacustrine systems developed in relatively young and tectonically active mountain belts record important information on high-frequency geological processes, despite their transient nature and poor preservation potential over geological times. Such basins indeed provide the unique opportunity to reconstruct the complex interplay between sedimentary and tectonic processes during the Holocene.

This is because the small intramontane lacustrine systems developed in tectonically active mountain belts record important information on high-frequency geological processes. The substrate on which these sedimentary systems develop is usually highly heterogeneous, consisting of low-grade metamorphic rocks represented by deformed, allochthonous accretionary complex lithologies. In particular, obducted ophiolites exhumed in many Alpine-Himalayan-type orogenic chains usually occur as lithoid blocks of various dimensions contained within argillaceous mélangé-type units due to subduction dynamics and mountain building processes [1–4]. Notably, this multiscale block-in-matrix arrangement strongly impacts the internal and external structural-stratigraphic architecture influencing slope stability, geological hazard, and surficial and groundwater flow [5–7]. In this framework, mountain lakes associated with small-scale catchment areas developed atop such ophiolite bodies with a clear structural control, given their close association with topographic lineaments [1,8,9].

This work investigates the upper Nure Valley, in the Emilia Apennines, dominated by the Mt. Ragola ophiolitic massif and strongly deformed clayey complexes belonging to External Ligurides Auctt. (Figure 1). In particular, coupled sedimentologic–paleoclimatic studies and small-scale basin analyses have been carried out in the Lake Moo deposits, implementing shallow coring and high-resolution radiocarbon dating [10], integrated with newly acquired geophysical profiling. These observations have been upscaled from the local to the regional scale and vice versa in order to achieve the most robust geological contextualization possible.

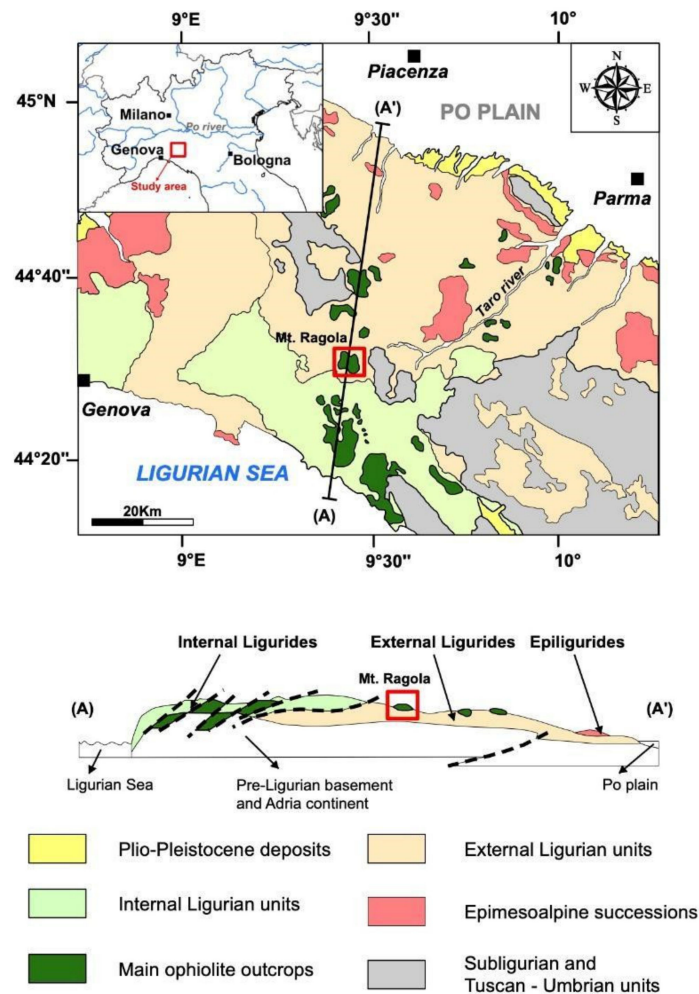


Figure 1. Tectonic sketch map and geological cross-section of the Northern Apennines (modified from [2]) with location of the study area (red box).

## 2. General Setting

The lithological background of the study area mainly consists of extensively deformed serpentinites in kilometer-sized masses that represent the accreted fragments of the Liguro-Piemontese oceanic basin separating the European and Adria plates during the Middle–Upper Jurassic [2–4].

In particular, Mt. Ragola (Lat. 44°38′30″N, Long. 10°5′E, 1712 m a.s.l.) consists of serpentinitized mantle tectonites [1] and appears as an orographic culmination of the External Ligurian units of the Northern Apennines (Figure 1). It is located about 45 km south of the town of Piacenza (Emilia-Romagna, Italy), in the Nure valley.

The ultramafic massif of Mt. Ragola (Figure 2) is extensively fractured, covers an area of about 24.2 km<sup>2</sup>, is about 300 m thick, and is bordered by low-permeability deposits that are predominantly characterized by polygenic breccias (Mt. Ragola Complex, Late Santonian Early Campanian [1]), made of heterometric blocks of limestones or marly limestones embedded in a fine-grained matrix (Figure 3). The base of the Mt. Ragola ophiolitic unit dips gently N–NE with a steepness of about 5% [1,11].

The geomorphology of the study area is highly heterogeneous, with scarps, ridges, gullies, and boulders emerging by selective erosion [1,12,13]. In particular, according to [13], the modern ophiolitic plate of Mt. Monte Ragola coincides with an original (paleo)structural low (graben) exhumed by unroofing and the differential erosion of the surrounding topographic highs made up by weaker argillaceous rocks, generating a geomorphic “inversion of relief”.

Erosional processes due to running water are widespread, with rills and gullies being the most common landforms in the ophiolitic rock mass due to surface water erosion.

They appear as systematic sets of linear features, usually eroded into the regolith covering the rock and into the bedrock. Generally, they give rise to networks of parallel, metric to decametric channels/trenches with limited hierarchy and are usually NW–SE and NE–SW oriented. Erosive scarps corresponding to the margins of weathering deposits appear heavily reshaped by running water and, to a lesser extent, by eluvial and colluvial deposits. The vast majority of these morphostructures and geomorphic features have been generally interpreted as the product of glacial action [1,12,13].

The geomorphological landscape also includes flat areas and steep slopes located at different altitudes. On the former, marshy environments commonly occur, recording the last filling phases of small lacustrine basins, some of which still exist at Lake Moo (Figure 4) and Lake Bino. The origin of these lakes is still a matter of debate as some authors have suggested a glacial origin [1,12,13], while others have interpreted the basin as the expression of Holocene deep-seated gravitational slope deformations (DSGSDs; [10,14]) mainly controlled by changes in the incision rates of the Nure stream and lateral valley unloading [1]. The complexity of past and present morphological processes is likely enhanced by the superposition of lithological units with strong mechanical contrast, such as ophiolites and the surrounding, predominantly clayey units [1].



**Figure 2.** Panoramic view of Mt. Ragola massif (1712 m a.s.l.) from the west side.

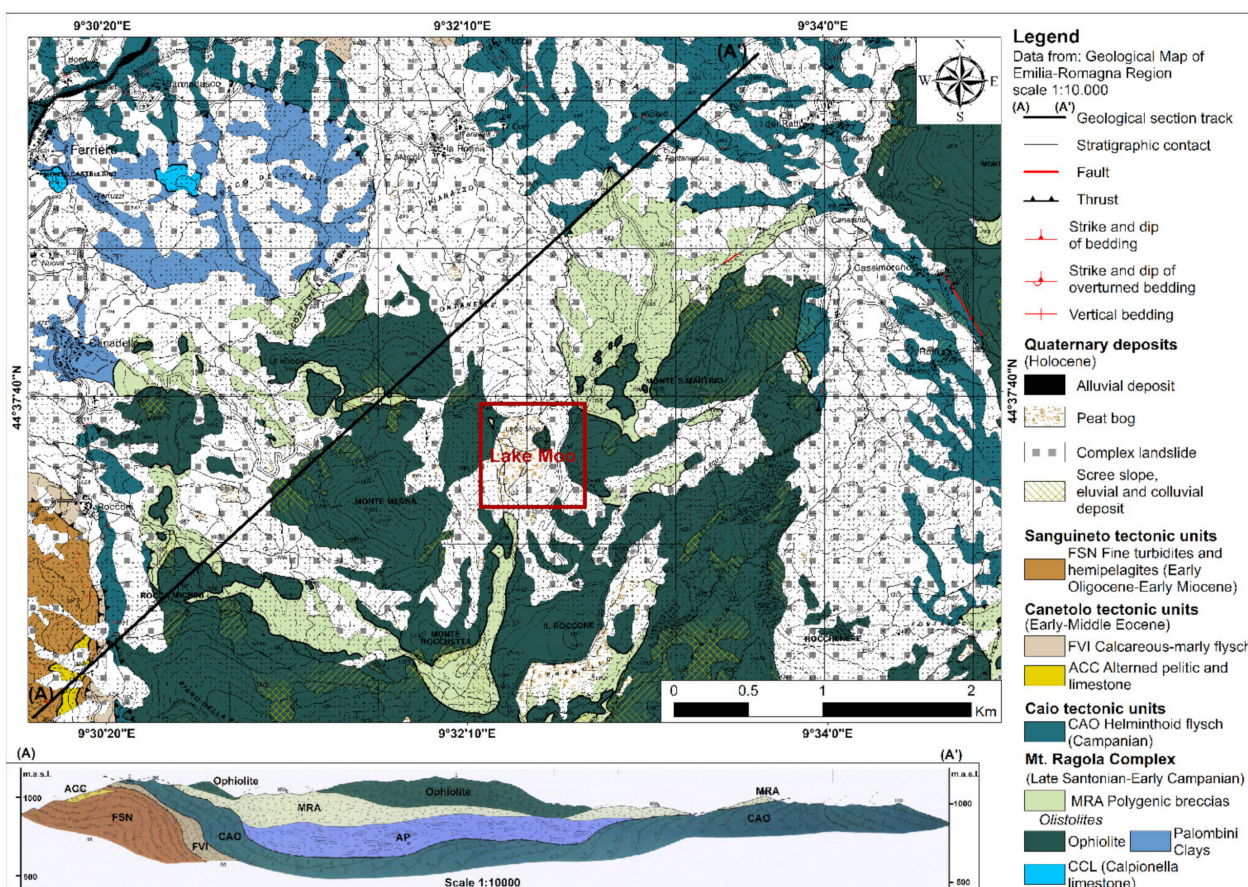


Figure 3. Map and geological cross-section of the Mt. Ragola ophiolitic massif with location of the study area. Modified from [11].



Figure 4. Panoramic view of the Lake Moo basin from the south.

Finally, it is worth mentioning that the area is included in the Natura 2000 network, code IT4020008—ZSC—Monte Ragola, Lago Moo, Lago Bino [15], and has been classified as a geological site of regional importance [16].

### 3. Materials and Methods

This work has been carried out integrating multiscale, geological and geomorphological data, both in time and space. This cross-disciplinary approach to the study of the Lake

Moo basin and surrounding area is described in the following paragraphs, from the small to the large scale.

At the local (basin) scale, we implemented:

- (a) Review of the following historical archives acquired by the Geological, Seismic, and Soil Service, reprocessed in GIS environment (georeferenced to the UTM system RER-ED50):
  - Color orthophotographs taken on 2006, [17];
  - Color orthophotographs taken on 2000, [17];
  - Black and white orthophotographs taken between the years 1994 to 1998, [17];
  - Black and white orthophotographs taken between the years 1988 to 1989, [17]; <http://www.pcn.minambiente.it/viewer/> (accessed on 27 June 2022)
  - Color aerial photographs at scale 1:13,000 taken between 1976 and 1978;
  - Black and white aerial photographs at scale 1:14,000 taken between 1969 and 1973;
  - Grayscale aerial photographs IGMI-GAI at scale 1:33,000, with 50 cm average pixel size, and pictures taken on July 1954 [18]; [https://servizimoka.regione.emilia-romagna.it/mokaApp/apps/VIGMIGAI1954\\_H5/index.html](https://servizimoka.regione.emilia-romagna.it/mokaApp/apps/VIGMIGAI1954_H5/index.html) (accessed on 27 June 2022) [https://servizimoka.regione.emilia-romagna.it/mokaApp/apps/VIGMIGAI1954\\_H5/index.html](https://servizimoka.regione.emilia-romagna.it/mokaApp/apps/VIGMIGAI1954_H5/index.html)
  - Historical aerial photographs acquired by Royal Air Force in Emilia-Romagna (1943–1944) [19];
  - Historical topographic maps (1860) of the Kingdom of Italy, called “I.G.M. primo impianto” and “I.G.M. secondo impianto” [18]; <https://servizimoka.regione.emilia-romagna.it/mokaApp/apps/CST2H5/index.html> (accessed on 27 June 2022) <https://servizimoka.regione.emilia-romagna.it/mokaApp/apps/CST2H5/index.html>
  - Map published by the Military Geographical Institute (I.G.M.) in the 1930s of the last century;
  - Historical topographic map of 1853 at scale 1:50,000 [18];
  - Historical topographic map of the Duchy of Parma of Piacenza of 1828 at scale 1:28,800 [18]; <https://servizimoka.regione.emilia-romagna.it/mokaApp/apps/CST1H5/index.html> (accessed on 27 June 2022)
- (b) A new UAV-based photogrammetric acquisition of the entire extension of the Lake Moo basin was performed in Summer 2021 with a 20 MP commercial-grade drone to obtain a 3D model tied to GIS-calibrated ground control points. From this 3D model, we extracted a high-resolution (ca. 1 cm) orthophotograph and DEM used as baseline for detailed mapping of scarps, vegetational/structural and spring alignments, and other geomorphic elements, which were subsequently carefully verified in the field.
- (c) A geoelectrical survey was carried out in Autumn 2021 to mainly determine the following:
  - Depth and geometry of the ophiolite bedrock;
  - Location of faults interacting with the bedrock and possibly with the sedimentary cover succession of the lake basin;
  - Subsurface depositional trends of sedimentary bodies.

The geophysical profiles follows a NE–SW direction and orthogonally intersects alluvial fan deposits and NW–SE structural lineaments identified through remote sensing observations. This survey was performed by making numerous apparent resistivity measurements employing quadripoles arranged along the selected profiles (2D) using 48 channel Electric Tomography, in conformity with the Wenner–Schlumberger electrode configuration method (after MH Loke—1997/2001), with a step of 5 m for a total length of 235 m. All the electrodes were georeferenced during the field survey. The obtained set of apparent resistivity values (pseudosections) were converted into actual ones by implementing the RES2DINV (version 3.5 4) of the Geotomo Software SDN BHD (Penang, Malaysia), allowing the construction of a two-dimensional resistivity model. A PASI Srl “POLARES 2.0” was used to carry out all resistivity measurements in the study area. The full database of the geoelectric survey and the technical specifications of the instrumentis are available

in Chapter 1 in Supplementary Materials. Previously published high-resolution reflection seismic data [20] were also used to backup and complement this dataset.

- (d) To investigate the sedimentary succession, two undisturbed sediment cores (T1 and T2) were acquired in summer 2019 in the Lake Moo plain using a Belarus peat corer [21] for a total of 7.5 m (T1, 3 m and T2, 4.5 m) and the lithofacies description is available in Chapter 2 in Supplementary Materials. Complementary data, obtained using a continuous drilling system described in [10] were also used. These data allow us to calibrate the geoelectric measurement data, establishing the resistivity range of various lithological units.
- (e) The chronostratigraphic framework was partly based on radiocarbon data from core S1 [10] integrated by two newly acquired radiocarbon ages obtained at the CEDAD Laboratory of the University of Salento (Italy). Original data are available in Chapter 3 in Supplementary Materials.

At the larger, regional scale we made use of the following:

- (a) Orthophotographs and DEM acquired by the Geological, Seismic, and Soil Service, analyzed in GIS environment (georeferenced to the UTM system RER-ED50), in particular, colored orthophotographs A.G.E.A., with a 30–50 cm average pixel size and pictures taken between May and June 2011, and June and August 2008, backed up by high-resolution colored UAV orthophotographs, specifically collected in June 2021. The workflow on DEM involved the outlining of topographic lineations using 4 illumination directions (0–90–180–270), sun position at 45°, and regular time intervals analysis, subsequently backed up by recognition of the same structures on aerial/UAV orthophotographs and directly on site. Saddles, scarps, crests, closed depressions, trenches, terraces, counter slope surfaces, hillbridges, vegetational alignments, and other elements were identified and mapped. The DEM used had a resolution of 5 m × 5 m cells.
- (b) Background geological data at the 1:10,000 scale, derived from the Emilia-Romagna Region database [22]. This database was integrated with an original geomorphological survey backed up by photointerpretation, and the results were carefully verified on site. The following complementary datasets and related interpretations from [23] were also used as baseline:
  - The morphometry of the hydrographic network, which evidenced a segmentation of the tributaries of the Nure river, interpreted as driven by mechanical discontinuities of the bedrock substrate;
  - The meso-structural analysis on brittle structures (e.g., faults, fractures) in the different lithological units, which highlighted the occurrence of tectonic lineaments and structural trends, interpreted as active also during the Holocene.
- (c) Finally, we reviewed the national earthquake catalog [24] to qualitatively identify possible relationships between epicentral clustering trends and structural patterns.

All territorial data are available in vector digital format, organized and managed in a database with two types of software: (1) ESRI 2018 ArcGIS 10.6.1 Redlands, CA Environmental Systems Research Institute. All this information is georeferenced in World Geodetic System 1984 (W.G.S. 84 datum). (2) A free and open-source geographic information system: QGIS 3.18 Zürich.

## 4. Data Analysis

### 4.1. Surface Data

The analysis of historical cartographic archives (Figure 5) allowed us to highlight the following main points:

- (a) In 1828 (Figure 5a), the main stream feeding Lake Moo was not following the current trend. On the contrary, it appeared to flow on the eastern side of the depression along a NE–SW direction.

- (b) In 1853 (Figure 5b), the stream was located in an intermediate position, flowing roughly in the middle of the depression. In 1860 (Figure 5c), the stream had already reached the current configuration in the western part of the basin, along a NW–SE direction that abruptly bent toward the East (with an angle of ca.  $90^\circ$ ) before entering into the lake.

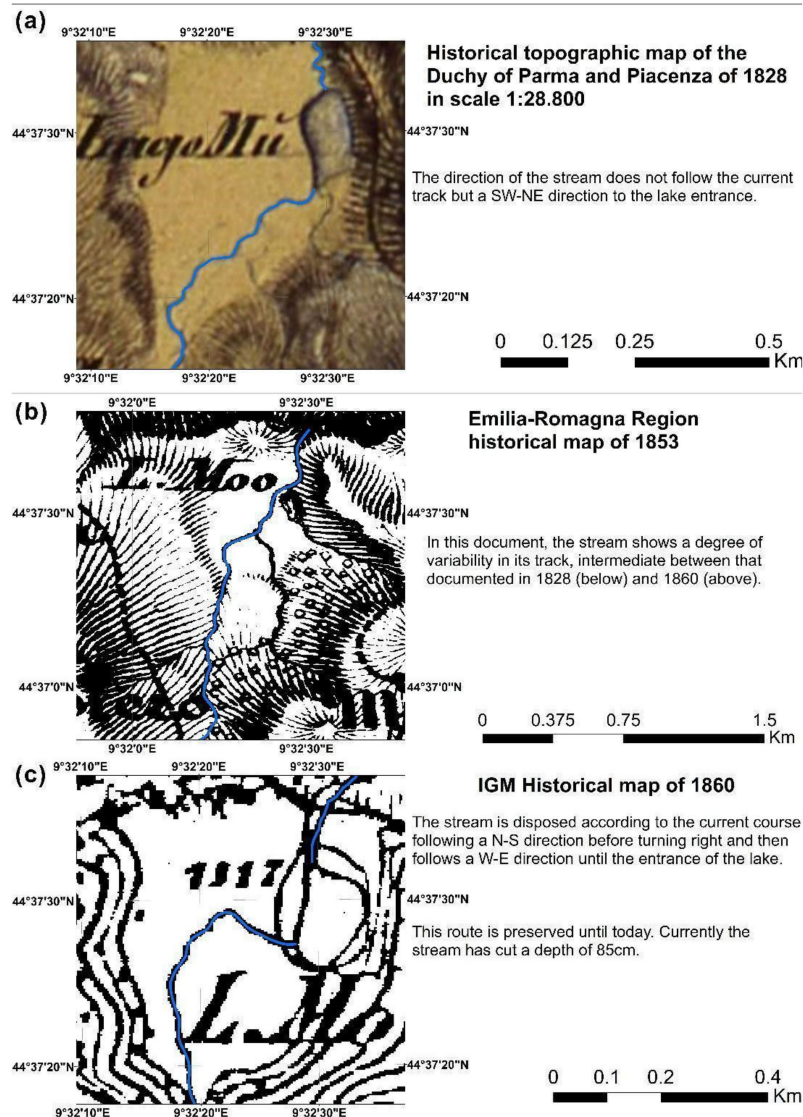


**Figure 5.** Historical cartography available for the study area. The blue line shows the different tracks of the main stream under study. (a) Historical topographic map of the Duchy of Parma and Piacenza of 1828 in scale 1:28,000; (b) Emilia-Romagna Region historical map of 1853; (c) IGM Historical map of 1860.

Analysis of the subsequent high-resolution datasets (aerial and satellite orthophotos, DEMs, topographic maps) acquired until the present day reveals that, after 1860, the stream maintained its current conformation. In particular, since then, there were no major changes in the general morphology of the entire Lake Moo basin. Currently, the stream riverbed shows a ca. 50 cm incision (Figure 6).

The identified inactive alluvial fan appears confined in the southern sector of the basin, being bounded to the north by a series of topographic lineaments directed NW–SE as illustrated in Figure 7. Such lineaments, expressed by cm- to dm-sized scarps, are clearly able to impact on the hydrographic network influencing the patterns of superficial rilling. In particular, groundwater spilling points within the Lake Moo basin follow these structural

trends as well. Notably, the coarse-grained lobe deposited during one of the most powerful and recent flood events (13–14 September 2015) appears to be confined to the southern part of the basin [10].



**Figure 6.** Representative photograph of the entrenched right side of the mainstream showing the uppermost 50-cm-thick sedimentary succession. Graded pebble–sand couplets are interpreted as a sheet-flood lobe deposit. Location in Figure 7.

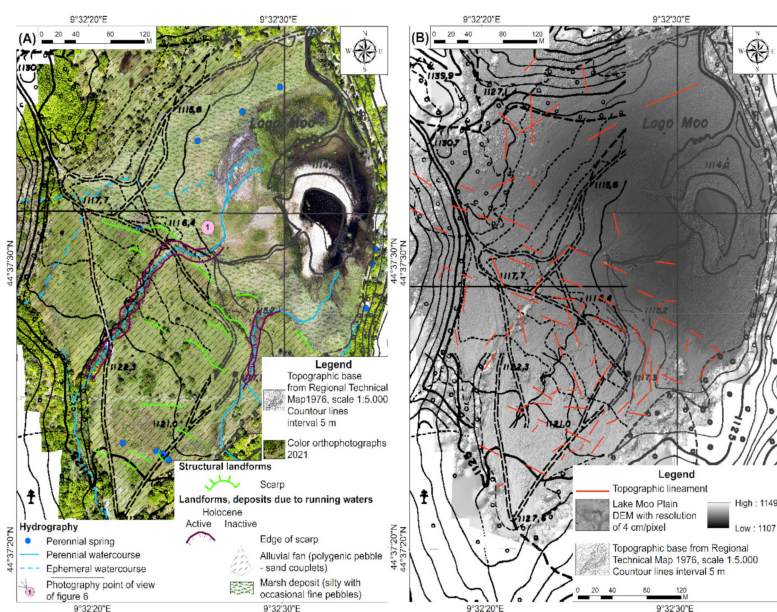


**Figure 7.** The main structural landforms and topographic lineament recognized in the lake Moo plain extracted from (A) high-resolution orthophotograph and (B) DEM, respectively.

#### 4.2. Subsurface Data

In order to validate and complement surface data, dedicated EM data was complemented and backed up by a reinterpretation of seismic tomography data acquired by previous campaigns [10]. The coverage of the geoelectric survey is shown in Figure 8. These profiles were specifically designed to cross the main morphostructures in N–S and E–W directions.

This allowed the identification of the possible contact between sediments and the bedrock at maximum and minimum depths of about 25 and 5 m, respectively, with a complex physiographic profile characterized by morphological highs and lows, roughly defining asymmetric depocenters, with shorter and steeper southern flanks compared to

the northern ones (Figure 8). The location and depth in meters from ground level of these structural highs and lows of the ophiolite substrate recognized through geoelectrical and seismic data are shown in Figure 8.

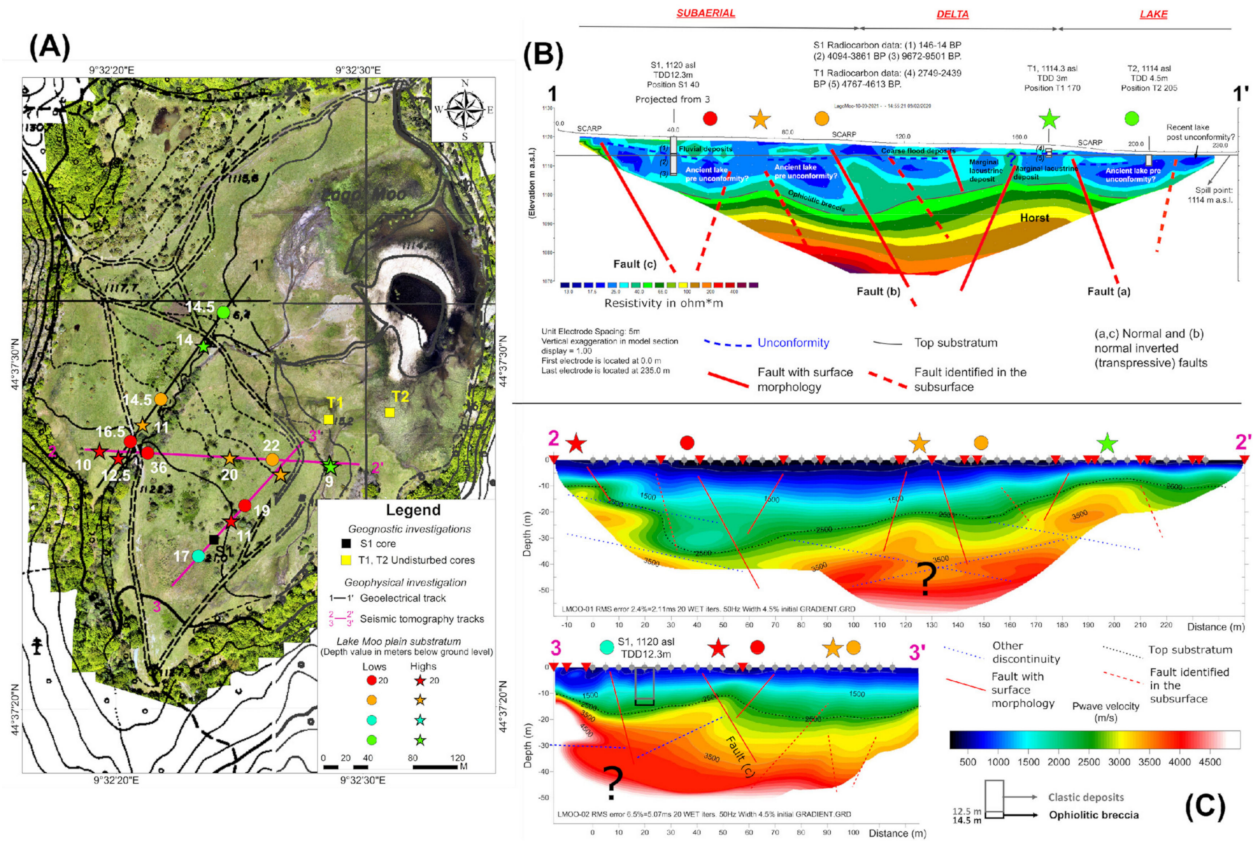


**Figure 8.** (A) Location of the geophysical profiles shown in (B,C) with labeling of the correlated structural highs and lows of the ophiolitic substrate. (B) Geoelectrical resistivity tomography and interpretation. The depth of the unconformity is in accordance with the spill point altitude of Lake Moo (1114 m a.s.l.). (C) Vp seismic tomography profiles (modified from [10], © Author(s) 2020, Creative Commons Attribution 4.0 License; <https://cp.copernicus.org/articles/16/1547/2020/cp-16-1547-2020-supplement.pdf>, accessed on 11 April 2022), and interpretation. Question marks outline areas with ambiguous and/or unclear results.

The base of the sedimentary sequence recognized in the geoelectrical profile was facilitated by information derived from the S1 core, where it is located at 12.5 m depth below ground level [10] and coincides with resistivity values ranging from 30 to 50  $\Omega \times m$ . Three principal lithologic subdivisions are recognized in the geoelectrical profile (see Chapter 1 in Supplementary Materials), and these subdivisions are in accordance with what was observed in core S1 [10]. In addition to the contact between the sedimentary sequence and ophiolitic breccias, through a sharp and erosive contact at a depth of 4.5 m, a transition occurs from shallow lacustrine clayey deposits with resistivity values below 25  $\Omega \times m$ , to a marginal lacustrine environment subject to flood deposits and subaerial very coarse sediments with resistivity values ranging between 25 and 40  $\Omega \times m$ . This limit corresponds to an important unconformity [10].

The calibration of the geophysical profiles is completed with two undisturbed sediment cores (T1 and T2, their location is shown in Figure 8 and see Chapter 3 in Supplementary Materials) taken in the northern sector of the lacustrine plain, where the most recent filling of the basin occurred. In this area, based on radiocarbon data, at a depth of 2.40 m, it was possible to recognize the unconformity surface that coincides with the erosive base of a 60-cm-thick graded layer (see Chapter 2 in Supplementary Materials) consisting

of coarse sandstone with very fine granules that transitions upward to siltstone with abundant remains of plant fragments. This coarse cluster was interpreted as the deposit from fluvial floods.

The tectonic discontinuities defining the structure of the subsurface framework are correlated in plan view with the NW–SE and NE–SW topographic alignments described above and are identified as aligned normal fault branches characterized by a local cumulative displacement of up to a few meters and a lateral extension of up to hundreds of meters. Such faults are arranged in arrays mainly N- and S-dipping, and W- and E-dipping, respectively, roughly defining an asymmetric horst-and-graben-type morphology in both directions. Several faults characterized by a surface expression (e.g., scarps up to ca. 30 cm high, vegetation and groundwater seepage alignment, stream diversions) have been correlated with the subsurface (see Figure 8). In particular, the NW–SE set appears to share the most evident topographic expression, also coinciding with the front of the alluvial fan. Two sets of low-angle mechanical discontinuities can be identified in the seismic tomographies, arranged as almost conjugate sets in the W–E profile (see Figure 8C).

#### 4.3. Large-Scale Surface Data

In plan view, the area surrounding the Lake Moo basin is characterized by a complex network of geomorphological features and drainage patterns (Figure 9). Closed and elongated depressions characterized by minor lakes, peat bogs, and humid areas such as the one hosting Lake Moo, are observed to align together with stream pathways, and other topographic lineaments, roughly defining a V-shaped, structurally controlled hydrographic network with the apex pointing toward SSW, where the local watershed is located, and draining toward the NNE, into the Nure valley. This structural framework is due to the development of a deep-seated gravity deformation of the slope [10,14], whose lateral margins/boundaries provide preferential pathways for two minor hydrographic basins comprising the Moo and Bino lacustrine basins (see Figure 9).

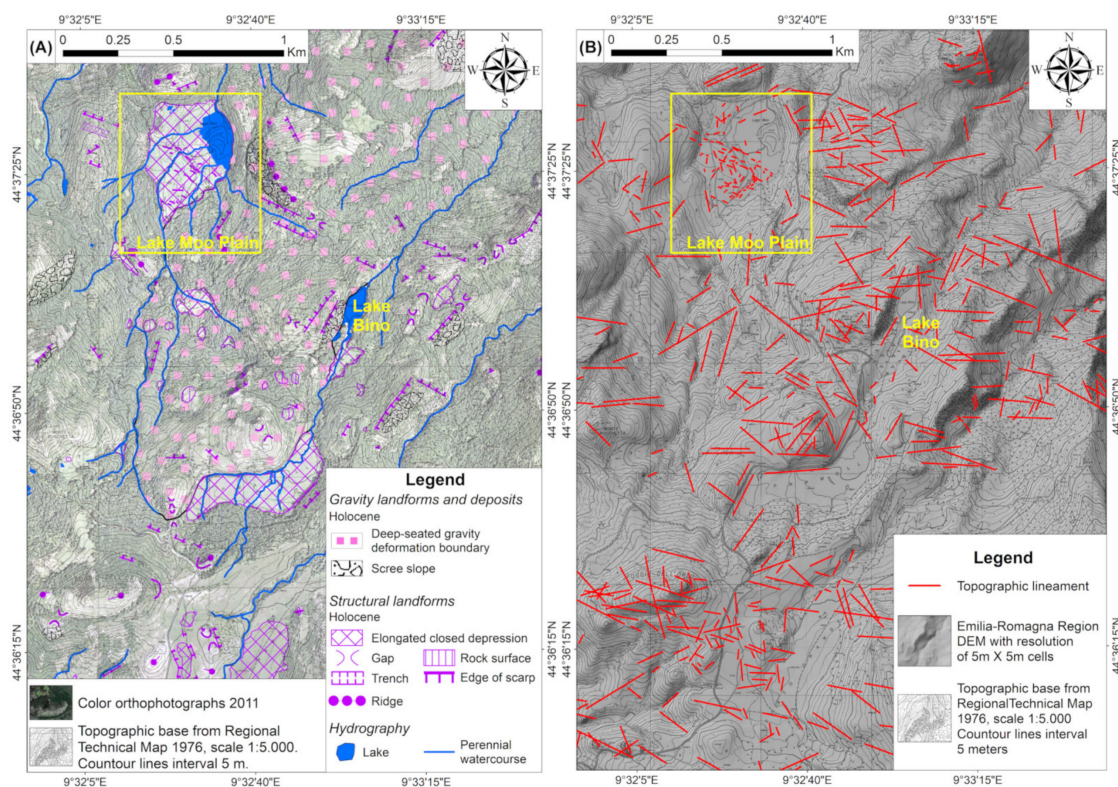


**Figure 9.** Main geomorphological features surrounding the study area. (A) Map of geomorphic structures. (B) Map of topographic lineaments.

Such basins appear elongated, together with other landforms (e.g., topographic depressions) and topographic alignments, in a NNE–SSW direction, following one of the main structural directions identified in the area. The other principal structural direction identified by different sets of the same morphostructures was WNW–ESE. These two structural populations show mutual crosscutting and abutting relationships.

## 5. Discussion

Combining surface and subsurface information allowed the identification of the subtle structural and stratigraphic relationships occurring in the Lake Moo basin and in the surrounding area. In particular, the coarse-grained coalescent lobes forming the alluvial fan that are structurally confined in the southern sector of the basin, lie upon an unconformity surface with a base dated 4094–3861 B.P. at 4.5 m depth (unconformity 1 in S1, Figure 8). As described above, such unconformity marks the abrupt upward transition between underlying lacustrine sediments to coarse-grained fluvial deposits [10] and appears shallower toward the north, being found at about 2 m depth in the footwall of fault A. To the northern part of the profile, unconformity 1 appears to get relatively deeper, again at 2–3 m depth in the hanging wall of fault A. This testifies to a stepped, asymmetric half-graben-type physiography, with compartmentalization of the original lake to the south and to the north of the main tectonic lineament discussed above, which appears to have played the role of a structural divisor/threshold (see Figures 7 and 8). As a whole, the stratigraphic depth of unconformity 1 coincides with the elevation of the spill point of Lake Moo, at 1114 m a.s.l. The same scenario appears in the E–W direction, with a deeper depocenter toward the west and a progressively shallower ophiolitic substrate toward the east, at least in the southern sector of the basin (i.e., to the south of the main NW–SE lineament; fault A in Figure 8B).

Based on these observations, the possible evolution of the Lake Moo basin can be subdivided into two main phases, defined by (1) a pre-unconformity succession, with the lacustrine basin subdivided into southern and northern depocenters, and (2) a post-unconformity phase, characterized by an abandonment of the southern part and shifting toward the north of the lacustrine basin depocenter to its current position. We interpret this shifting as related to the activity of an array of mainly high-angled, oblique normal faults with local transtensive (and sometimes transpressive or inverted) movements dipping mostly toward the north (see Figures 7 and 8), which can be followed outside the investigated area, showing a strong correspondence with the local to regional structural grain (Figure 9), as also documented in the literature [13,23].

Notably, as illustrated in Figure 10, the 1860 time interval coincides with the last peak of the Little Ice Age [25]. Accordingly, the observed changes in the riverbed trends and overall drainage system of the Lake Moo basin could be interpreted as consequences of a series of floods that occurred between 1828 and 1860, characterized by cold and humid climatic conditions [26]. This reconstruction on the basis of cartographic documentation of a period of regularly intense precipitation coinciding with the last peak of the Little Ice Age is in accordance with what is also documented in other historical sources, where it is recorded, for example, that at least three intense precipitation events with disastrous flooding occurred between late September and October 1868 in the Alpine sector [27] and in the Northern Apennines [28]. In particular, the flood of 23rd September 1868 had such an impact on the city of Parma that the “Stuard Gallery” exhibits a painting with the disastrous effects on the city caused by the waters of the Parma stream [29]. The coarse-grained sedimentary lobes deposited by such floods are localized at the slope break, where the stream enters the lake basin. These deposits form an alluvial fan characterized by a steepness of about 4.4% and 2.6° of inclination. According to the above framework, we suggest that along with the W–E asymmetry of the basin, the resultant topographic expression of this fan might have been able to modify the stream path, steering it toward the west (see Figure 5).

These alluvial fan deposits identified are limited to the southern sector of the Lake Moo plain, being bounded to the north by a series of topographic lineaments directed NW–SE as

illustrated in Figure 7. These lineaments, identified in the field as vegetational alignments, scarps with decimetric-sized relief, and by rectangular drainage patterns, intersect a large-scale deep-seated gravity movement guided by a set of other lineaments oriented NE–SW (see Figure 9). In the apical sector, both the Moo and Bino lakes appear located on both sides of the gravity movement (Figure 11). Their position along the lateral, NE–SW-oriented ramps of the DSGSD, along with their symmetric rhomboidal-shaped appearance (suggesting opposite shear sense as expected at the side of the gravity movement), testify to a common transtensional (i.e., pull-apart type) origin for both lacustrine basins (see Figure 11).

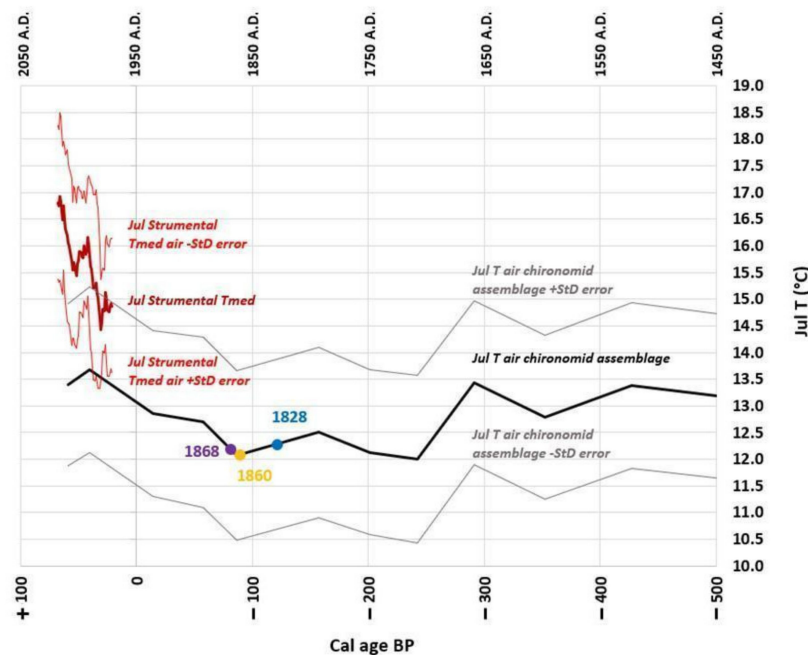


**Figure 10.** The black line shows the reconstructed temperature, while the gray lines are the sample-specific estimated standard error associated with the temperature reconstruction based on chironomid assemblages from [24]. The dark red line represents the July mean temperature (1971–2018) retrieved for the Verdaroło meteorological station of ARP Ae-SIMC network Emilia-Romagna Region (11-year running average). The light red lines are standard deviation error.

This possible gravitational origin of the two lakes is in agreement with what was observed in the S1 borehole extracted at the Lake Moo plain in July 2017 [10], where at a depth between 12.25 and 11.30 m, a 95-cm-thick unit composed of two main horizons indicative of a mature paleosol occurred. The lowermost horizon, located between 12.25 and 11.60 m, corresponds to weathered deposits overlain by a 30-cm-thick horizon. This unit is interpreted as a residual pedogenized colluvium marking the base of a structural depression produced by gravitational block sliding [10]. At the top of the paleosol, at a depth of 10.44 m, a level of organic matter was dated 9672–9501 B.P., which could represent the initiation phase of the gravitational destabilization that subsequently continued during the Holocene Climatic Optimum.

This initial phase of the Mt. Ragola landslide destabilization is in accordance with what is described in the Northern Apennines by [30] and by [31] in the Alps system as a consequence of evolution of the geological slope system to reactions of climate changes that occurred during the transition between the late Boreal and early Holocene Climatic Optimum periods. In the study area, this slope evolution is favored by the superposition of intensely fractured lithological units with strong mechanical contrast, such as ophiolites, and the underlying a predominantly clayey unit, mainly controlled by changes in the incision rates of the Nure stream and the tectonic uplift of the Apennine chain during the Holocene [1,13,23]. Moreover, the intrinsic foliation systems of the serpentinites seem to

provide favorably oriented weak surfaces for the development of the basal detachment of the DSGSD (see Figure 11). According to this framework, the transpressive reactivation shown by some faults can be related to local inversions that occurred during the stepwise evolution of the DSGSD.

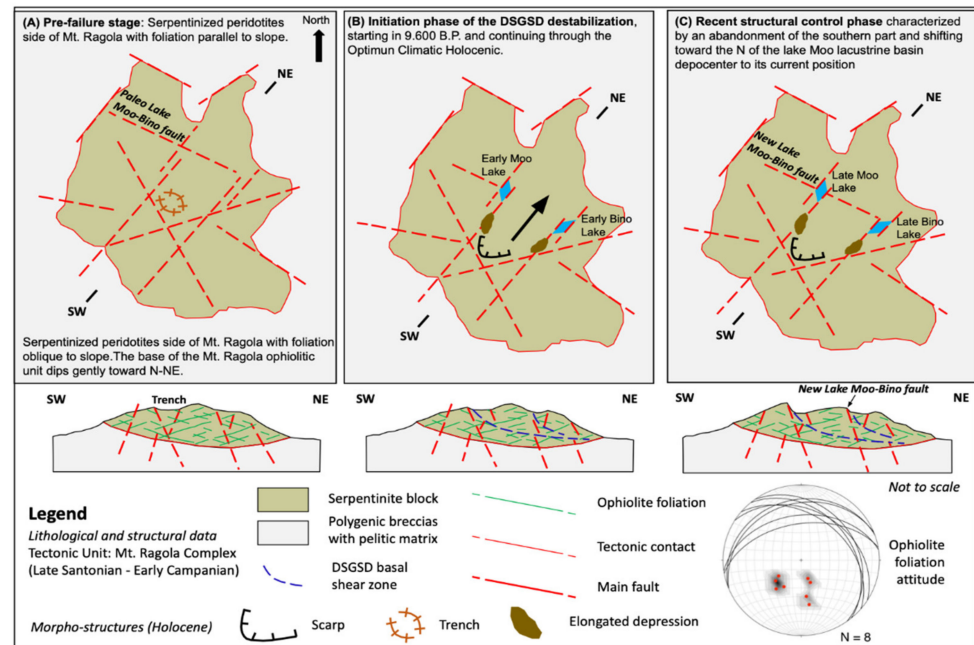


**Figure 11.** Synthetic conceptual model showing the origin and subsequent evolution of the Moo and Bino lakes. (A) Pre-failure stage: Serpentinized peridotites side of Mt. Ragola with foliation parallel to slope; (B) Initiation phase of the DSGSD destabilization, starting in 9.600 B.P. and continuing through the Holocene Climatic Optimum; (C) Recent structural control phase characterized by an abandonment of the southern part and shifting toward the N of the lake Moo lacustrine basin depocenter to its current position.

As depicted in Figure 9, the surface of the deep-seated gravity movement complex and its structures are crosscut by geomorphologic elements such as aligned trenches, saddles, scarps, vegetational lineaments, and interruptions of elongated structural highs and lows, characterized by lateral continuity outside the lacustrine basin. Based on the coherent geometric relationships of such elements with the regional topographic lineaments identified within (see Figure 7) and around the Lake Moo basin (see Figure 9), we suggest their tectonic origin. In this framework, these geomorphological elements appear related to the recent activity of this fault array, which post-dates the gravity movement. Importantly, this fault system seems to be related to the recent reactivation of older tectonic structures, with the same geometric attitude, interpreted as responsible for the development and lateral compartmentalization of the deep-seated gravity movement (see Figure 11) and, more generally, of the structural architecture of the Mt. Ragola massif.

This scenario is supported by the literature, as studies carried out in the late 1980s documented several faults in the area sharing a recent activity [13,23,32]. In particular, structural investigations suggested the occurrence of three deformational phases, two of which were characterized by the transcurrent regime trending NE–SW and NNW–SSE, respectively, and a third, younger distensive one. The latter developed two normal fault systems, trending NE–SW (monodirectional extension) and NW–SE (pluridirectional extension), with local transpressive movements [23].

Finally, it is worth noting that a good match exists between these structural features, the trend of the potentially active faults previously mapped in the area, and the alignment and cluster trends of the epicenters of historical earthquakes (Figure 12). Overlying this

integrated information on the overall regional seismotectonic setting in fact allows correlation of the identified morphostructures and recently active tectonic lineaments, trending NW–SE, NE–SW, and NNE–SSW and mainly characterized by normal oblique slip and strike-slip movements. Notably normal and dextral strike slip focal mechanisms were extrapolated for clusters of seismic events (from  $2 \leq M \leq 4.4$ ) aligned along a NW–SE lineament that intersects the Lake Moo basin [23]. This structure is interpreted as responsible for the linear topographic features and, in synergy with the climatic scenario described above, for the segmentation of the lacustrine basin. It is worth noting that the period of increased flood activity recorded between 1820 and 1870 coincides with a temporal cluster of  $M > 3$  seismic events, characterized by at least two  $M > 5.5$  major ones that occurred within a radius of 50 km of the study area (see chronological earthquake distribution in Figure 12).

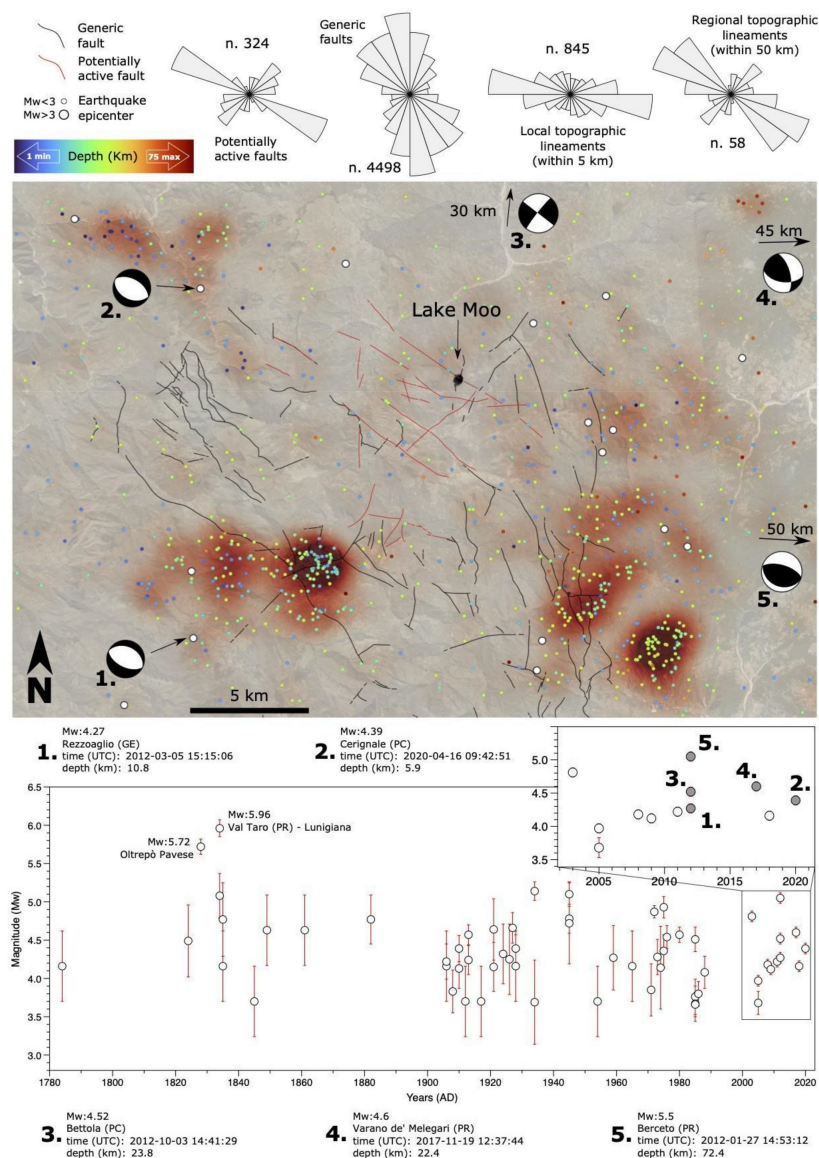


**Figure 12.** Heatmap overlay of earthquake epicenters, color coded by depth (time interval 1541–2021; [24]), on Google Earth satellite imagery of the area surrounding the Lake Moo basin, with rose diagrams summarizing the main structural orientations. Generic fault and potentially active fault data from [1] and [23], respectively. In the bottom diagram, chronological distribution of historical  $M > 3$  seismic events occurred in an area of 50 km radius around Lake Moo. Data from [24]. The main  $M > 4$  earthquakes with available reconstructed focal mechanisms are labeled.

## 6. Conclusions

The multidisciplinary approach implemented in this work allowed a detailed characterization of the Lake Moo basin, its evolution through geological to historical times, and the reconstruction of a possible chronology of the geomorphological development of the study area within the Northern Apennines framework. Analysis of historical archives, geophysical surveys, geognostic probing, radiocarbon dating, and geological and geomorphological mapping allowed the reconstruction of the tectonic–climatic evolution of this sector of the Northern Apennines during the Holocene.

In particular, this study allowed us to disregard the glacial origin classically proposed for this lacustrine basin, instead revealing that a combination of relatively recent sedimentary, gravitational, and (neo)tectonic processes played a major role in the morphological reshaping of the study area. In the last 10 Kyr, the overall depositional setting appears structurally controlled, characterized by shifts of the equilibrium point (i.e., balance between erosion and deposition). Three main processes linked by a synergic loop were responsible for the morphological reshaping of the area:

- (1) Enhanced efficiency of regular fluvial discharge in humid and cold climatic conditions at the demise of the Little Ice Age;
- (2) Deep-seated slope gravity deformation due to tectonic uplift, unroofing, and lateral valley unloading;
- (3) Temporal–spatial clustering of seismic events along specific directions parallel to the local to regional structural grain.

The resultant physiographic scenario, which is preconditioned by the subsurface geological architecture, is mainly driven by lithological/mechanical contrast and reworking/reactivation of inherited structures.

In this framework, the (geo)diversity of the high Northern Apennines landscape can provide the constraints for a detailed assessment of the present and future geomorphic hazards for the local communities, as well as potential guidelines for the local governance of land management, planning, and safety. The proposed multidisciplinary analytical workflow highlights the importance of minor mountain lake environments and peat bogs as high-resolution geological archives. Such an approach might be implemented in other similar settings, characterized by limited outcrop conditions due to active tectonics, complex argillaceous lithologies, and/or unfavorable vegetation cover.

**Supplementary Materials:** The following supporting information can be downloaded at <https://www.mdpi.com/article/10.3390/geosciences12070272/s1>: Figure S1. Tomographic profile location “ERT L1”; Figure S2. Georesistivity meter “Polares 2.0”; of PASI Srl, employed for the geoelectric survey; Figure S3. Technical specifications of the “POLARES 2.0”; used for the geoelectric survey; Figure S4. Documentation of fieldwork activities; Figure S5. Documentation of fieldwork activities; Figure S6. ERT L1 Resistivity; Figure S7. ERT L1 Chargeability; Figure S8. ERT L1 Comparison between resistivity (top) and block sensitivity (bottom); Figure S9. ERT L1 Comparison between resistivity (top) and block uncertainty (bottom); Figure S10. ERT L1 Comparison between min and max resistivity models; Figure S11. ERT L1 Comparison between resistivity and chargeability; Figure S12. ERT L1 Comparison between resistivity and chargeability and interpretation; Figure S13. T1 core: main sedimentological features and lithofacies characterization; Figure S14. T2 core: main sedimentological features and lithofacies characterization; Figure S15. T1 core: position of the sampled at the depth between 130–133 cm for radiocarbon dating (A) and between 237–240 cm (B); Figure S16. Calibration of the conventional radiocarbon date of samples LTL20417A and LTL20418A; Table S1. Data Summary; Table S2. Full list of Radiocarbon sample age and description details.

**Author Contributions:** Conceptualization, S.S. and K.O.; methodology, S.S. and K.O.; software and created the figures, S.S., K.O., G.O. and S.G.; field data acquisition and curation, S.S., K.O., S.G., G.O., L.F.M. and M.C.; writing—original draft preparation, S.S. and K.O.; writing—review and editing, S.S., K.O., L.F.M. and L.M.; project management and coordination, S.S. and K.O. All authors have read and agreed to the published version of the manuscript.

**Funding:** This research received no external funding.

**Acknowledgments:** We would like to thank Editors Ashley Zhang and Sorin Hadrian Petrescu, and three anonymous reviewers for their constructive criticism, comments and suggestions. Thanks to Federico Grazzini (ARPAe-SIMC Emilia-Romagna Region) for the instrumental data to complete Figure 10. The T1 and T2 peat cores were obtained using a Belarus peat corer kindly made available by the MUSE of Trento (Marco Cantonati and Nicola Angeli). A special thanks to Stefano Tavani (University of Naples Federico II) for his help in the structural interpretations during the revision.

**Conflicts of Interest:** The authors declare no conflict of interest.

## References

1. Elter, P.; Ghiselli, F.; Marroni, M.; Ottria, G. *Note Illustrative del Foglio 197 “Bobbio” della Carta Geologica d’Italia alla Scala 1:50.000*; Istituto Poligrafico e Zecca dello Stato: Rome, Italy, 1997; pp. 1–106.
2. Marroni, M.; Meneghini, F.; Pandolfi, L. Anatomy of the Ligure-Piemontese subduction system: Evidence from Late Cretaceous-middle Eocene convergent margin deposits in the Northern Apennines, Italy. *Int. Geol. Rev.* **2010**, *52*, 1160–1192. [[CrossRef](#)]
3. Marroni, M.; Meneghini, F.; Pandolfi, L. A revised subduction inception model to explain the Late Cretaceous, double-vergent orogeny in the precollisional western Tethys: Evidence from the Northern Apennines. *Tectonics* **2017**, *36*, 2227–2249. [[CrossRef](#)]
4. Molli, G. Northern Apennine-Corsica orogenic system: An updated overview. *Geol. Soc. Lond. Spec. Publ.* **2008**, *298*, 413–442. [[CrossRef](#)]
5. Segadelli, S.; Vescovi, P.; Ogata, K.; Chelli, A.; Zanini, A.; Boschetti, T.; Petrella, E.; Toscani, L.; Gargini, A.; Celico, F. A conceptual hydrogeological model of ophiolitic aquifers (serpentinised peridotite): The test example of Mt. Prinzera (Northern Italy). *Hydrol. Processes* **2016**, *32*, 969–1201. [[CrossRef](#)]
6. Segadelli, S.; Vescovi, P.; Chelli, A.; Petrella, E.; De Nardo, M.T.; Gargini, A.; Celico, F. Hydrogeological mapping of heterogeneous and multi-layered ophiolitic aquifers (Mountain Prinzera, northern Apennines, Italy). *J. Maps* **2017**, *13*, 737–746. [[CrossRef](#)]
7. Segadelli, S.; Filippini, M.; Monti, A.; Celico, F.; Gargini, A. Estimation of recharge in mountain hard-rock aquifers based on discrete spring discharge monitoring during base-flow recession. *Hydrogeol. J.* **2021**, *29*, 949–961. [[CrossRef](#)]
8. Chelli, A.; Segadelli, S.; Vescovi, P.; Tellini, C. Large-scale geomorphological mapping as a tool to detect structural features: The case of Mt. Prinzera ophiolite rock mass (Northern Apennines, Italy). *J. Maps* **2016**, *12*, 770–776. [[CrossRef](#)]
9. Mariani, G.S.; Zerboni, A. Surface Geomorphological Features of Deep-Seated Gravitational Slope Deformations: A Look to the Role of Lithostructure (N Apennines, Italy). *Geosciences* **2020**, *10*, 334. [[CrossRef](#)]
10. Segadelli, S.; Grazzini, F.; Rossi, V.; Aguzzi, M.; Marvelli, S.; Marchesini, M.; Chelli, A.; Francese, R.; De Nardo, M.T.; Nanni, S. Changes in high-intensity precipitation on the northern Apennines (Italy) as revealed by multidisciplinary data over the last 9000 years. *Clim. Past* **2020**, *16*, 1547–1564. [[CrossRef](#)]
11. Ghiselli, G.; Marroni, M.; Ottria, G.; Zecca, P. *Carta Geologica dell’Appennino Emiliano-Romagnolo 1:10.000, Sezione 197150 Ferriere Est*; Regione Emilia-Romagna, SELCA stampe: Florence, Italy, 1999.
12. Marchetti, G.; Fraccia, R. Carta geomorfologica dell’alta Val Nure, Appennino piacentino. Scala 1:25.000. In *Il Paesaggio Fisico dell’Alto Appennino Emiliano*, 1st ed.; Carton, A., Panizza, M., Eds.; Grafis Edizioni: Bologna, Italy, 1988; pp. 95–120.
13. Carton, A.; Panizza, M. *Il Paesaggio Fisico dell’Alto Appennino Emiliano*, 1st ed.; Grafis Edizioni: Bologna, Italy, 1988; p. 182.
14. Geological, Soil and Seismic Survey of the Emilia-Romagna Region. Available online: [https://geo.regione.emilia-romagna.it/cartografia\\_sgss/user/viewer.jsp?service=geologia](https://geo.regione.emilia-romagna.it/cartografia_sgss/user/viewer.jsp?service=geologia) (accessed on 29 March 2022).
15. Protected Areas, Natura 2000 Network and Forests. Available online: <https://ambiente.regione.emilia-romagna.it/it/parchi-natura2000/rete-natura-2000/siti/it4020008> (accessed on 27 January 2022).
16. Geosites and Geological Heritage. Available online: <https://geo.regione.emilia-romagna.it/schede/geositi/scheda.jsp?id=2140> (accessed on 21 January 2022).
17. Geoportale Nazionale. Available online: <http://www.pcn.minambiente.it/viewer/> (accessed on 28 June 2022).
18. Servizio Moka Regione Emilia-Romagna. Available online: [https://servizimoka.regione.emilia-romagna.it/mokaApp/apps/VIGMIGAI1954\\_H5/index.html](https://servizimoka.regione.emilia-romagna.it/mokaApp/apps/VIGMIGAI1954_H5/index.html) (accessed on 28 June 2022).
19. Geoportale Regione Emilia-Romagna. Available online: <https://geoportale.regione.emilia-romagna.it/applicazioni-gis/regione-emilia-romagna/cartografia-di-base/cartografia-storica> (accessed on 28 June 2022).
20. Original High-Resolution Reflection Seismic Data. Available online: <https://cp.copernicus.org/articles/16/1547/2020/cp-16-1547-2020-supplement.pdf> (accessed on 29 March 2022).
21. Jowsey, P.C. An improved peat sampler. *New Phytol.* **1966**, *65*, 245–248. [[CrossRef](#)]
22. Geological cartography webgis. Available online: [https://ambiente.regione.emilia-romagna.it/en/geologia/cartography/webgis/geological-cartography-webgis?set\\_language=en](https://ambiente.regione.emilia-romagna.it/en/geologia/cartography/webgis/geological-cartography-webgis?set_language=en) (accessed on 29 March 2022).
23. Perotti, C.R.; Savazzi, G.; Vercesi, P.L. Evoluzione morfotettonica recente della zona compresa tra la testata del T. Nure e la Val d’Aveto (Appennino piacentino). *Suppl. Geogr. Fis. Dinam. Quat.* **1988**, *1*, 121–140. Available online: [http://www.glaciologia.it/wp-content/uploads/Supplementi/FullText/SGFDQ\\_I\\_1988\\_FullText/12\\_SGFDQ\\_I\\_1988\\_Perotti\\_121\\_140.pdf](http://www.glaciologia.it/wp-content/uploads/Supplementi/FullText/SGFDQ_I_1988_FullText/12_SGFDQ_I_1988_Perotti_121_140.pdf) (accessed on 27 June 2022).
24. Rovida, A.; Locati, M.; Camassi, R.; Lolli, B.; Gasperini, P.; Antonucci, A. (Eds.) *Italian Parametric Earthquake Catalogue (CPTI15); Version 4.0*; Istituto Nazionale di Geofisica e Vulcanologia (INGV): Rome, Italy, 2022. [[CrossRef](#)]

25. Samartin, S.; Heiri, O.; Joos, F.; Renssen, H.; Franke, J.; Brönnimann, S.; Tinner, W. Warm Mediterranean mid-Holocene summers inferred from fossil midge assemblages. *Nat. Geosci.* **2017**, *10*, 207–212. [[CrossRef](#)]
26. Soldati, M.; Borgatti, L.; Cavallin, A.; De Amicis, M.; Frigerio, S.; Giardino, M.; Mortara, G.; Pellegrini, G.B.; Ravazzi, C.; Surian, N.; et al. Geomorphological evolution of slopes and climate changes in northern Italy during the late Quaternary: Spatial and temporal distribution of landslides and landscape sensitivity implications. *Geogr. Fis. E Din. Quat.* **2006**, *29*, 165–183.
27. Brönnimann, S.; Rohr, C.; Stucki, P.; Summermatter, S.; Bandhauer, M.; Barton, Y.; Fischer, A.; Froidevaux, P.; Germann, U.; Grosjean, M.; et al. 1868—L'alluvione che cambiò la Svizzera: Cause, conseguenze e insegnamenti per il futuro. *Geogr. Bernensia* **2018**, *94*, 52. [[CrossRef](#)]
28. Giannecchini, R.; D'Amato Avanzi, G. Historical research as a tool in estimating hydrogeological hazard in a typical small alpine-like area: The example of the Versilia River basin (Apuan Alps, Italy). *Phys. Chem. Earth* **2012**, *49*, 32–43. [[CrossRef](#)]
29. Stuard Gallery. Available online: <https://complessopilotta.it/opera/i-guasti-dellinondazione-di-parma-del-1868/> (accessed on 29 March 2022).
30. Bertolini, G.; Pizziolo, M. Risk assessment strategies for the reactivation of earth flows in the Northern Apennines (Italy). *Eng. Geol.* **2008**, *102*, 178–192. [[CrossRef](#)]
31. Le Roux, L.; Schwartz, S.; Gamond, J.F.; Jongmans, D.; Bourles, D.; Braucher, R.; Mahaney, W.; Carcaillet, J.; Leanni, L. CRE dating on the head scarp of a major landslide (Séchilienne, French Alps), age constraints on Holocene kinematics. *Earth Plan. Sci. Lett.* **2009**, *280*, 236–245. [[CrossRef](#)]
32. Barbano, D.; Perotti, C.; Vercesi, P.L. La tettonica recente dell'alta Val Nure (PC). *Atti Ist. Geol. Univ. Pavia* **1984**, *30*, 221–233.